Progress of Theoretical Physics, Vol. 64, No. 2, August 1980

Quantization of Magnetic Excitation Continuum Due to Interchain Coupling in Nearly One-Dimensional Ising-Like Antiferromagnets

Hiroyuki SHIBA

Institute for Solid State Physics, University of Tokyo, Tokyo 106

(Received March 10, 1980)

The transverse magnetic excitation continuum of purely one-dimensional Ising-like antiferromagnets is formed from one magnon state and the odd-number-magnon (3-magnon, 5-magnon, $\cdots$) bound states, which are mixed by the off-diagonal exchange interaction. The interchain molecular field causes a decoupling of these bound states and leads to quantization of the excitation continuum. This quantization effect can explain fine structures of magnon Raman spectrum of $CsCoCl_3$ and $CsCoBr_3$, which have been observed recently at low temperatures and remain unexplained so far.

§ 1. Introduction

The excitation spectrum in one-dimensional (1D) spin systems has been a subject of considerable experimental and theoretical interest.[1] In a previous paper,[2] which will be referred to as IS, we proposed a theory of magnetic excitation line shape for 1D spin $\frac{1}{2}$ Ising-like antiferromagnets (AF):

$$\begin{aligned}\mathcal{H}_0 &= 2J\sum_j [S_j^z S_{j+1}^z + \varepsilon (S_j^x S_{j+1}^x + S_j^y S_{j+1}^y)] \\ &\equiv \mathcal{H}_{zz} + \mathcal{H}_{xy}\,, \end{aligned} \tag{1}$$

where ε is assumed to be small. The ε term in (1) removes the high degeneracy of the energy spectrum of the pure Ising model ($\varepsilon = 0$). This effect leads to propagating domain walls (solitons)[3] and to the magnetic excitation continuum in transverse (S^x and S^y) spin fluctuation spectrum.[2] The theoretical studies of the model (1) are expected to be useful to understand $CsCoCl_3$[4] and $CsCoBr_3$,[5] which are believed to be typical 1D Ising-like AF's.[4)~7)] Recent neutron scattering experiments[8),9)] on $CsCoCl_3$, in particular, have revealed the transverse magnetic excitation continuum, whose line shape is asymmetric in energy and whose width becomes small at antiferromagnetic Brillouin zone boundary. This result for the line shape is consistent with the prediction of IS.

The purpose of this paper is to extend IS to low temperature region by taking the interchain coupling into account. We show, first, that the molecular field of neighboring chains causes *quantization of the excitation continuum* and leads to a *series of discrete lines* below 3D ordering temperature. As we will show, this is mathematically an analogue of *Stark ladder* of 1D tight-binding electrons

in a uniform electric field;[10] therefore we call this quantization effect *Zeeman ladder*.

Secondly we wish to propose the Zeeman ladder as an explanation of a series of discrete lines of "magnon" spectrum, which has recently been observed in $CsCoCl_3$[11),12)] below the 3D ordering temperature with high-resolution Raman spectroscopy. The magnon Raman spectrum of $CsCoBr_3$[13)] shows similar discrete lines at low temperatures.

This paper is arranged as follows: In § 2 the effect of interchain coupling on the magnetic excitation continuum is studied and the concept of Zeeman ladder is explained. In § 3 the theory of Zeeman ladder is applied to interpret magnon Raman spectra in $CsCoCl_3$ at low temperatures. A summary is given in § 4. In order to estimate the magnitude of interchain coupling, the 3D ordering of $CsCoCl_3$ and $CsCoBr_3$ is described in the Appendix by treating the intrachain Ising interaction exactly and the interchain coupling in the molecular field approximation.[14)]

§ 2. Effect of interchain molecular field on the transverse magnetic excitation continuum

Let us study the magnetic excitation spectrum of nearly 1D spin $\frac{1}{2}$ Ising-like AF, taking a weak interchain coupling into account. Our model Hamiltonian is then $\mathcal{H}=\sum_\lambda \mathcal{H}_0{}^{(\lambda)}+\sum_{\lambda,\mu}\mathcal{H}_1{}^{(\lambda,\mu)}$ where $\mathcal{H}_0(\lambda)$ is the intrachain Hamiltonian (1) of the λ-th chain and $\mathcal{H}_1{}^{(\lambda,\mu)}$ represents the interchain coupling between nearest neighbor chains:

$$\mathcal{H}_1{}^{(\lambda,\mu)}=2\sum_{(j,l)} J'\left(S^z_{j\lambda}S^z_{l\mu}+\varepsilon'\left(S^x_{j\lambda}S^x_{l\mu}+S^y_{j\lambda}S^y_{l\mu}\right)\right). \tag{2}$$

$\sum_{(\lambda,\mu)}$ and $\sum_{(j,l)}$ denote a summation over nearest neighbor chain pairs and nearest neighbor intrachain spin pairs, respectively. In the case of $CsCoCl_3$ and $CsCoBr_3$ the anisotropy of the exchange interaction comes mainly from the anisotropy of wave function in the lowest Kramers doublet[4)] so that $\varepsilon'\sim\varepsilon$ is expected. Since ε is estimated as $\varepsilon\sim 0.1$ for those materials, the $\varepsilon' J'$ term in (2) may be ignored in a first approximation. If we treat the remaining Ising interchain interaction in (2) in the molecular field approximation, we are led to the following effective single-chain Hamiltonian:

$$\mathcal{H}=\mathcal{H}_0+\mathcal{H}', \tag{3}$$

where $\mathcal{H}_0$ is given by (1) and

$$\mathcal{H}'=-\sum_j h_j S_j{}^z \tag{4}$$

with $h_j=(-1)^j\cdot h$ $(h\geq 0)$. Having $CsCoCl_3$ and $CsCoBr_3$ in mind, we assume h and εJ are much smaller than J.

An extension of the perturbation theory of IS to include the molecular field term (4) is straightforward. In order to make the present paper self-contained, however, we repeat partly the argument in IS. Up to first order of ε the ground state $|g\rangle$ of (3) is simply

$$|g\rangle \simeq \Psi_{\text{Neel 1}} - \frac{1}{2J}\mathcal{H}_{XY}\Psi_{\text{Neel 1}}, \tag{5}$$

where $\Psi_{\text{Neel 1}}$ is one of the two Neel states, which is favorable under the staggered field h, and $2J+2h$ has been approximated by $2J$. The excited states with $S^z=1$, which are separated from the ground state by $\sim 2J$, consist of

$$\begin{cases} \Psi_1(k) = \sqrt{\dfrac{2}{N}} \sum\limits_j e^{ikR_j} S_j^+ \Psi_{\text{Neel 1}} + O(\varepsilon), \\ \Psi_3(k) = \sqrt{\dfrac{2}{N}} \sum\limits_j e^{ikR_j} S_j^+ S_{j+1}^- S_{j+2}^+ \Psi_{\text{Neel 1}} + O(\varepsilon), \\ \qquad \cdots\cdots\cdots\cdots \\ \Psi_{N-1}(k) = \sqrt{\dfrac{2}{N}} \sum\limits_j e^{ikR_j} S_j^+ \prod\limits_{\nu=1}^{(N/2)-1} (S_{j+2\nu-1}^- S_{j+2\nu}^+) \Psi_{\text{Neel 1}} + O(\varepsilon). \end{cases} \tag{6}$$

The corresponding excited states with $S^z=-1$ are obtained from (6) by interchanging S^+ and S^-. Clearly Ψ_3, Ψ_5, $\cdots$ are 3-magnon, 5-magnon, $\cdots$ bound states respectively.*) The matrix elements of $\mathcal{H}$ within (6) have the form**)

$$\begin{aligned} &\langle \Psi_{2\nu-1}(k) | \mathcal{H} | \Psi_{2\nu'-1}(k) \rangle \\ &= \begin{cases} 2J\left(1+\dfrac{3}{2}\varepsilon^2 - \dfrac{1}{2}\varepsilon^2\delta_{\nu,1}\right) + 2(2\nu-1)h & \text{for } \nu'=\nu \\ V_1 & \text{for } \nu'=\nu+1 \\ V_1^* & \text{for } \nu'=\nu-1 \\ V_2 & \text{for } \nu'=\nu+2 \\ V_2^* & \text{for } \nu'=\nu-2 \\ 0 & \text{otherwise} \end{cases} \\ &\equiv (\nu | \hat{H}(k) | \nu'), \end{aligned} \tag{7}$$

where $V_1 = \varepsilon J(1+e^{-2ika})$ and $V_2 = -\frac{1}{2}\varepsilon^2 J(1+e^{-4ika})$. Here the diagonal terms are measured from the energy of the Neel state $\Psi_{\text{Neel 1}}$: $E_0 = -N(\frac{1}{2}J(1+\varepsilon^2)+\frac{1}{2}h)$.

*) The even-number-magnon (2-magnon, 4-magnon,$\cdots$) bound states belonging to $S^z=0$ also give rise to excitations around $2J$, which appear as a weak continuum in $S_{zz}(Q;\omega)$.[2]

**) Here we calculate the excitation energy up to second order of ε. The second order term does not change the first order result qualitatively; however we have included the second order term to compare the theoretical spectrum quantitatively with the experiment.

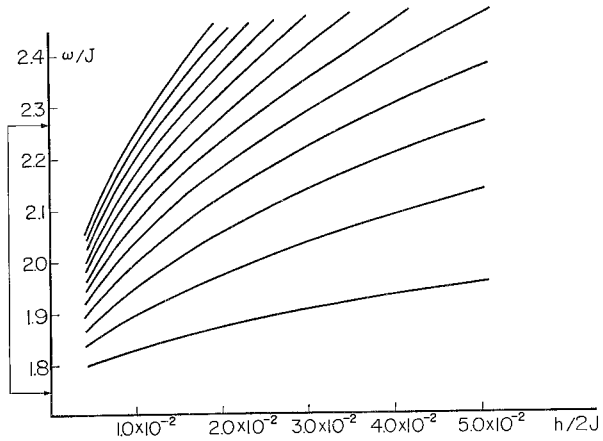

Fig. 1. Energy spectrum of magnetic excitation (7) for $ka=0$ or π as a function of interchain molecular field h. ε is chosen as 0.13. The levels higher than the 12-th are omitted here. The region indicated by the arrows is the continuum for $h=0$.

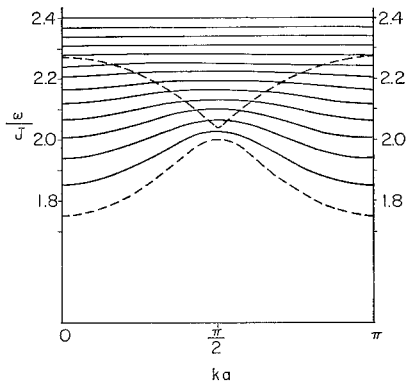

Fig. 2. Energy spectrum of (7) as a function of ka. The energy levels higher than 2.4 are omitted here. $h/2J=1.5\times10^{-2}$ and $\varepsilon=0.13$ are chosen. The broken lines show the excitation continuum for $h=0$.

One notices immediately that (7) is equivalent to the Hamiltonian matrix of *1D tight-binding electron in a uniform electric field*; V_1, V_2 and h are then interpreted as nearest and next nearest neighbor transfer matrix and the electric field, respectively. The solution of the latter problem is well known:[10] In the absence of the electric field the energy spectrum consists of a continuum due to band motions, while the uniform electric field quantizes the continuum into discrete levels, which are often called "Stark ladder". Therefore the magnetic excitation continuum[2),15),16)] of purely 1D Ising-like AF is also quantized under the molecular field into discrete levels, which we call "Zeeman ladder".

The energy spectrum of (7) for $ka=0$ or π has been evaluated numerically and is shown in Fig. 1 as a function of $h/2J$ by assuming $\varepsilon=0.13$.*) As is well known in the Stark-ladder problem the level separation of low energy lines is not constant, but decreases with increasing energy. Figure 2 shows the wave vector dependence of energy levels for nonzero h; the continuum of energy spectrum for $h=0$ is also shown for comparison.

The transverse magnetic excitation line shape for $T=0$°K can be obtained from

$$S_{xx}(Q,\omega)=\sum_f |\langle f|S_Q^x|g\rangle|^2\delta(\omega-E_f+E_g), \tag{8}$$

where $|g\rangle$ and $|f\rangle$ are the ground state and an excited state of the system, respectively; E_g and E_f are corresponding energies. As shown in IS, using the

*) This value was chosen here because IS's analysis[2)] of the spin wave spectrum[7)] in $CsCoCl_3$ led to $\varepsilon=0.13$.

perturbational wave functions (5) and (6), one finds for $S_{xx}(Q, \omega)$ the following expression:

$$S_{xx}(Q, \omega) \simeq -\frac{1}{4\pi} \mathrm{Im}\Big[(1-\varepsilon \cos Qa)^2 G(1,1) - (1-\varepsilon \cos Qa)\left(\frac{V_1^*}{2J} G(1,2) + \frac{V_1}{2J} G(2,1)\right) + O(\varepsilon^2)\Big], \tag{9}$$

where

$$G(\nu, \nu') = \left(\nu \left| \frac{1}{\omega - \hat{H}(Q) + i\delta} \right| \nu'\right) \quad (\delta \to +0) \tag{10}$$

is the Green's function defined with (7). If the eigenfunctions of $\hat{H}(Q)$ defined by $\hat{H}(Q)|\psi_\lambda\rangle = E_\lambda |\psi_\lambda\rangle$ are used, (9) may be written as

$$S_{xx}(Q, \omega) \simeq \frac{1}{4} \sum_\lambda \delta(\omega - E_\lambda)\left[(1-\varepsilon \cos Qa)^2 |(1|\psi_\lambda)|^2 - 2(1-\varepsilon \cos Qa)\,\mathrm{Re}\{(2|\psi_\lambda)(1|\psi_\lambda)^*\} + O(\varepsilon^2)\right]. \tag{11}$$

Thus we can easily evaluate $S_{xx}(Q, \omega)$ from the diagonalization of $\hat{H}(Q)$; Fig. 3 shows an example of the results. Notice that the intensity is the largest for the lowest-energy line and that it decreases in a monotonic way with the energy increased. This feature can be explained as follows: The magnetic excitation for $h=0$ forms a continuum because odd-number-magnon bound states, Ψ_3, Ψ_5, $\cdots$ in (6), are equal in energy, if $\varepsilon=0$, to the single magnon state Ψ_1, and mix well with each other for $\varepsilon \neq 0$. Under a finite interchain molecular field ($h>0$), however, magnon bound states cost more energy than Ψ_1 so that the main part of the magnetic excitation intensity is concentrated on the lowest line having the largest Ψ_1 component. For a large h the weak side lines appearing in the energy region higher than the lowest-energy line may be regarded as magnon bound state lines, which are slightly mixed with each other and with Ψ_1.

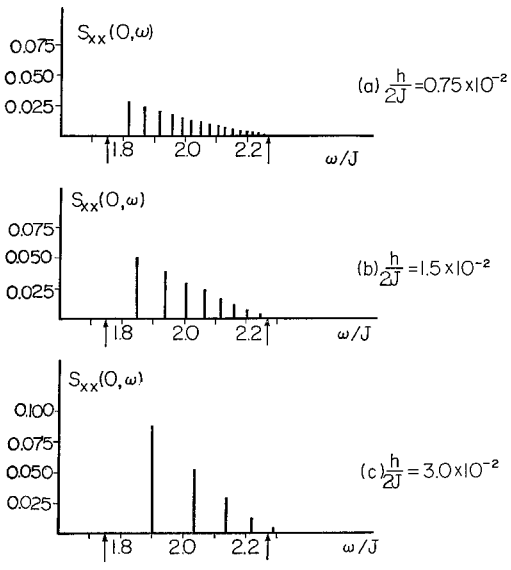

Fig. 3. $S_{xx}(Qa=0, \omega)$ as a function of ω/J. $h/2J$ is chosen as (a) 0.75×10^{-2}, (b) 1.5×10^{-2} and (c) 3.0×10^{-2}. The arrows indicate the region of excitation continuum expected for $h=0$.

Let us point out in this connection that the Zeeman ladder proposed

in this paper is closely related to the multiple-magnon bound states in nearly 1D Ising-like *ferromagnets* ($CoCl_2 \cdot 2H_2O$, etc.).[17),18)] As we have already seen, the Zeeman ladder is the multiple-magnon bound states in nearly 1D Ising-like *antiferromagnets*. An important difference is that the off-diagonal term of the exchange interaction can mix the multiple-magnon bound states well in the AF's since they belong to the same S^z. Thus the mixing due to the εJ term shows up clearly in the spectrum. On the other hand, in the F's the bound states belong to different S^z states so that they do not mix with each other.

§ 3. Interpretation of fine structures of magnon Raman spectra in $CsCoCl_3$

As we have already pointed out in § 1, recent high-resolution magnon Raman scattering in $CsCoCl_3$[11),12)] is remarkable in that it shows a number of sharp lines at low temperatures, i.e., below 3D ordering temperature. The Raman experiment on $CsCoBr_3$[13)] also shows discrete lines, which have presumably the same origin as those in $CsCoCl_3$. These two AF's are known to have two ordered phases: low temperature phase at $T<T_{N2}$ ($T_{N2}=8°K$[11)] or 9.2°K[7)] for $CsCoCl_3$ and $T_{N2}=10\sim14°K$[5)] for $CsCoBr_3$) and intermediate phase at $T_{N2}<T<T_{N1}$ ($T_{N1}=21.3°K$[7)] for $CsCoCl_3$ and $T_{N1}=28.3°K$[5)] for $CsCoBr_3$). According to Mekata[19)] they are "ferrimagnetic" and "antiferromagnetic" phases, which are shown in Fig. 4. Here we shall propose an interpretation of discrete lines in low-temperature Raman spectra on the basis of Zeeman ladder and Mekata's assignment of magnetic phases. We shall focus our discussion mainly on $CsCoCl_3$ for which high resolution data are available.

The magnon Raman spectra of $CsCoCl_3$,[11),12)] whose peak position is listed in Table I, have the following features:

[F1] The magnetic-field dependence of these lines shows that they are magnetic excitations changing S^z by unity. Therefore a possibility of "two-magnon" Raman scattering is excluded.

[F2] For $T<T_{N2}$ 3 strong lines (series A) and several weak lines (series B) are observed.

[F3] For $T_{N2}<T<T_{N1}$ the intensity of series B grows up remarkably and the relative intensity of series B and series A is reversed.

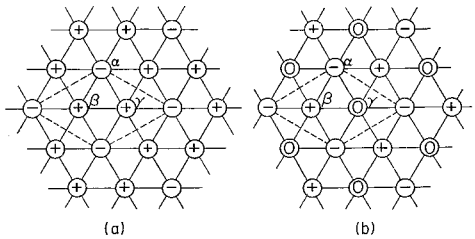

Fig. 4. Magnetic ordering[19)] of $CsCoCl_3$ and $CsCoBr_3$ for (a) $T<T_{N2}$ and for (b) $T_{N2}<T<T_{N1}$. + and − denote up and down spins, while 0 represents a paramagnetic chain.

Table I.

magnon Raman line (cm^{-1})	proposed assignment			calculated (cm^{-1})		
85.6			B_2			86.3
88.8		B_1			90.3	
90.5	A			93.6		
94.3			B_2			93.0
100.1			B_2			98.4
101.0		B_1			100.9	
105.0			B_2			103.2
106.6	A			107.2		
109.0			B_2			107.4
110.0		B_1			109.1	
112.9			B_2			111.4
116.3	A	B_1		117.4	116.1	

Table II.

	molecular field h	weight	assignment
$T<T_{N2}$	$6J_1'$	$\frac{1}{3}$	A
	0	$\frac{2}{3}$	C
$T_{N2}<T<T_{N1}$	$6J_1'$	$\frac{1}{8}\times\frac{2}{3}=\frac{1}{12}$	A
	$4J_1'$	$\frac{3}{8}\times\frac{2}{3}=\frac{1}{4}$	B_1
	$2J_1'$	$\frac{3}{8}\times\frac{2}{3}=\frac{1}{4}$	B_2
	0	$\frac{1}{3}+\frac{1}{12}=\frac{5}{12}$	C

[F4] The peak position of lines at $T_{N2}<T<T_{N1}$ is, within the experimental accuracy, the same as that at $T<T_{N2}$.

[F5] In the series A the lowest-energy peak has the largest intensity. In the series B the lowest-energy two peaks are the strongest lines.

[F6] These discrete lines are superposed on a plateau, which extends from $\sim$80 cm^{-1} to $\sim$120 cm^{-1}.

Before going into analysis we have to estimate the magnitude of various magnetic interactions in $CsCoCl_3$. The intrachain interaction is estimated as $J\sim 75°K$[7] and $\varepsilon\sim 0.13$.[2] Interchain Ising interaction can be estimated from T_{N2} and T_{N1} by assuming antiferromagnetic nearest-neighbor chain interaction (J_1') and ferromagnetic next nearest neighbor chain interaction (J_2'). We applied to this problem the molecular field theory,[14] which takes into account the intrachain Ising interac-

tion exactly and the interchain interactions in the mean field approximation. It is described in the Appendix, where J_1' and J_2' are estimated as $J_1'/J \sim 0.6 \times 10^{-2}$ and $J_2'/J_1' \sim 10^{-2}$. Therefore we conclude that the main interchain coupling is the nearest neighbor antiferromagnetic Ising interaction J_1'. The off-diagonal term of interchain exchange interaction is smaller than J_1' by factor of $\varepsilon(\sim 0.1)$ as noted in § 2. Thus the magnetic excitations in $CsCoCl_3$ may be regarded, in a good approximation, as confined in each chain so that we apply our theory for $S_{xx}(Q, \omega)$ to the Raman experiment by taking $Qa=0$. Neutron scattering[6] did not see any dispersion of magnons perpendicular to the chain, which is consistent with the present model.

Let us explain theoretically the peak position of Raman lines and the temperature dependence of the intensity on the basis of the following model:

(A) For $T<T_{N2}$ one third of the total chains (denoted by α in Fig. 4(a)), surrounded by six AF nearest neighbor chains give the lines of series A; the remaining two thirds (denoted by β and γ), to which the molecular field h due to n.n. chains cancels, give rise to excitation continuum, i.e., plateau.

(B) For $T_{N2}<T<T_{N1}$ one third of the total chains (denoted by γ in Fig. 4(b)) remain paramagnetic[17] so that we regard the spins on γ chains as taking up or down state with the probability 1/2 for each without any correlation to other chains.*) Thus the molecular field h to α and β chains takes 0, $2J_1'$, $4J_1'$, or $6J_1'$ with the probability $\frac{1}{8}$, $\frac{3}{8}$, $\frac{3}{8}$, or $\frac{1}{8}$ respectively; the molecular field to γ chains is zero.

Our model predicts for $T<T_{N2}$ one series of discrete lines (assigned as series A) and a continuum. On the other hand, for $T_{N2}<T<T_{N1}$, we have three series of discrete lines (assigned as series A, B_1 and B_2) and a continuum. In this way the present model can give a simple explanation of complicated 12 lines. The result is summarized in Table II. The assignment of series A is unique; the assignment of series B to series B_1 and B_2 in Table I has been made by comparing theoretical line splitting (shown in Fig. 1) with observed line position and intensity of series B. To calculate the theoretical line position we have changed J_1' to make a fit to the observed twelve lines with the J value fixed at 75°K. Among several trials we show a typical result corresponding to $J_1'/J=0.96\times10^{-2}$; the calculated line position for this case is shown in Table I. J_1' is the only parameter for fitting the absolute position of the twelve lines so that the overall agree-

*) The correlation length $\xi(T)$ $(\sim ae^{J/kT})$ along the "paramagnetic" chain as well as the characteristic time of spin flipping τ in the chain $(\sim(\varepsilon J)^{-1}\hbar\xi(T)/a)$ is large for $T \ll J$. Therefore it is expected that for $T \ll J$ the random molecular field Δh $(\sim J_1')$ due to the "paramagnetic" chain has an almost constant saturation value over a large distance $(\sim\xi)$ and changes its sign only occasionally $(\sim 1/\tau)$. According to a general theory of line shape[18] the effect of the random molecular field on the spectrum can be regarded as static when $\Delta h\tau > \hbar$ is satisfied. Thus the present treatment is justified when $\Delta h\tau/\hbar \sim (J_1'/\varepsilon J)e^{J/kT} > 1$, i.e., $T < J/k \ \ln(\varepsilon J/J_1') \sim 24$°K using $\varepsilon \sim 0.13$ and $J_1'/J \sim 0.6\times10^{-2}$.

ment is encouraging. In particular the features [F1]$\sim$[F6], which we pointed out before, are in accord with the present model. Let us make some additional comments:

[1] Several weak lines (series B) for $T<T_{N2}$ are explained as magnetic excitations at domain boundaries of possible three domains, where chains with $h=2J_1$ and $4J_1'$ are present.*)

[2] The states with $S^z=-1$, which are obtained from (6) by interchanging S^+ with S^- also give the same spectrum as (6) so that every line is doubly degenerate for zero external magnetic field. Zeeman splitting is expected for a finite field. Therefore this model can explain [F1] easily.

[3] According to our assignment the series B_1 and B_2 have the same weight, which is three times as large as series A. This is in agreement with the observed intensity (compare three lines at 86.5, 88.8 and 90.5 cm^{-1}).

[4] In each series of A, B_1 and B_2 the line intensity decreases in a monotonic way with the increase of energy. This is again what the present theory predicts.

[5] To regard the interchain molecular field as static is justified, as noted before, for $\Delta h\cdot\tau/\hbar>1$, where $\Delta h\sim J_1'$ and $\tau\sim(\hbar/\varepsilon J)\,e^{J/kT}$. When $\Delta h\tau/\hbar$ becomes smaller than unity with the increase of temperature, the Zeeman ladder cannot be resolved due to averaging of the molecular field by rapid fluctuations. We do not expect any sharp change of Raman line shape at T_{N1}.

Although the present model can explain a number of features of the Raman experiment, there remain some unanswered questions:

[1] According to Refs. 11) and 12), once the magnon Raman peaks shifted to high energy by the external field cross the E_{1g} phonon line at 118 cm^{-1}, the peaks disappear and cannot be traced. The present author does not have any explanation for this.

[2] The present theory predicts three series of lines whose intensity decreases in a monotonic way for each series. The Raman experiment seems to show that the lines around 116 cm^{-1} are fairly strong. It might be due to an accidental overlap of lines belonging to different series. If this is not the case, a new mechanism is required to explain this phenomenon.

Let us discuss briefly the recent Raman experiment on $CsCoBr_3$[13], which is believed to have magnetic properties similar to $CsCoCl_3$. Although the resolution of the data is not so good as in Refs. 11) and 12), the spectra at the lowest temperature 8.5°K ($<T_{N2}$) do show a series of discrete lines. The position is 100.5, 111.5, 123.7, 133 and 141 cm^{-1}. We tentatively assign these lines as corresponding to series A in $CsCoCl_3$. We note that the Raman spectrum reported for 49°K shows an asymmetric broad line shape, which is similar to $S_{xx}(\Omega a=0,\omega)$

*) In the case of nearly 1D Ising-like ferromagnet, which is a counterpart of the present AF, magnetic excitations at domain boundaries have been observed.[21]

calculated in IS. More work is certainly needed on $CsCoBr_3$.

§ 4. Summary

It is widely accepted that magnetic excitations form a continuum in purely 1D quantum-mechanical spin $\frac{1}{2}$ antiferromagnets. In the Ising-like case the physical picture of this continuum is clear: The continuum consists of one-magnon state and odd-number-magnon (3-magnon, 5-magnon, ···) bound states, which are mixed up with each other by the ε term of (1). We have shown that a weak interchain molecular field tends to decouple these multiple-magnon bound states; it results in a series of discrete lines, which we call Zeeman ladder in analogy with Stark ladder of 1D tight-binding electrons in a uniform electric field. We have also shown that this Zeeman ladder is capable of explaining complicated magnon Raman lines reported on $CsCoCl_3$ and $CsCoBr_3$.

Acknowledgements

The author is indebted to Professor K. Hirakawa, Professor J. Kanamori, Professor Y. Endoh and Mr. H. Yoshizawa for useful discussions and to Dr. G. Shirane for informing him of unpublished data as well as for valuable correspondence. This work is supported by Grant-in-Aid of Ministry of Education, Science and Culture.

Appendix

—Theory of Magnetic Ordering in $CsCoCl_3$ and $CsCoBr_3$—

Mekata[19] developed a theory of magnetic ordering in $CsCoCl_3$ and $CsCoBr_3$ by using a two-dimensional model (i.e., by assuming the intrachain correlation length is infinite). He could explain the nature of low temperature phase ($T<T_{N2}$) as well as intermediate phase ($T_{N2}<T<T_{N1}$). In order to estimate the magnitude of interchain coupling from T_{N1} and T_{N2}, however, the two-dimensional model is insufficient. Here we apply to this problem Scalapino-Imry-Pincus theory,[14] in which the intrachain interaction is taken into account exactly and the interchain coupling is treated in the mean field approximation. This approximation is expected to be adequate if 3D ordering temperature is much lower than intrachain coupling strength.

We start with the following model:

$$\mathcal{H}=2J\sum_{\lambda}\sum_{j}S^z_{j\lambda}S^z_{j+1\lambda}+2J_1'\sum_{\lambda,\mu}^{n.n}\sum_{j}S^z_{j\lambda}S^z_{j\mu}+2J_2'\sum_{\lambda,\mu}^{n.n.n}\sum_{j}S^z_{j\lambda}S^z_{j\mu}\,, \qquad (\mathrm{A}\cdot 1)$$

where the three terms represent intrachain, nearest neighbor chain and next nearest neighbor chain couplings, respectively. $J>0$, $J_1'>0$ and $J_2'<0$ are assumed in (A·1).

The small off-diagonal exchange term has been ignored in the intrachain term. It is important for discussing dynamics, but is expected to give a small correction to thermodynamic properties. Having three sublattices shown in Fig. 4 in mind, we apply the mean field approximation to (A·1) as

$$\mathcal{H}\simeq 2J\sum_{\lambda}\sum_{j}S^{z}_{j\lambda}S^{z}_{j+1\lambda}+6J_1'\sum_{\lambda}\sum_{j}S^{z}_{j\lambda}(\langle S^{z}_{j\lambda'}\rangle+\langle S^{z}_{j\lambda''}\rangle+\alpha\langle S^{z}_{j\lambda}\rangle)$$
$$-3J_1'\sum_{\lambda}\sum_{j}\langle S^{z}_{j\lambda}\rangle(\langle S^{z}_{j\lambda'}\rangle+\langle S^{z}_{j\lambda''}\rangle+\alpha\langle S^{z}_{j\lambda}\rangle), \quad (A\cdot 2)$$

where $\alpha=2J_2'/J_1'$ and $(\lambda,\lambda',\lambda'')$ denote three different sublattices. (A·2) can be solved by the well-known exact solution of 1D Ising model. Introducing the sublattice magnetizations as

$$\langle S^{z}_{j\lambda}\rangle=(-1)^{j}\cdot\frac{1}{2}\langle\sigma_1\rangle,\quad \langle S^{z}_{j\lambda'}\rangle=(-1)^{j}\cdot\frac{1}{2}\langle\sigma_2\rangle,\quad \langle S^{z}_{j\lambda''}\rangle=(-1)^{j}\cdot\frac{1}{2}\langle\sigma_3\rangle,$$

we obtain the following self-consistency equations:

$$\langle\sigma_i\rangle=f(K,L_i), \quad (A\cdot 3)$$

where $K=J/kT$ and $f(x,y)=e^{x}\mathrm{sh}\ y/\sqrt{1+(e^{x}\mathrm{sh}\ y)^2}$. The L's are defined as

$$\begin{cases} L_1=-\dfrac{3J_1'}{2kT}(\langle\sigma_2\rangle+\langle\sigma_3\rangle+\alpha\langle\sigma_1\rangle), \\ L_2=-\dfrac{3J_1'}{2kT}(\langle\sigma_3\rangle+\langle\sigma_1\rangle+\alpha\langle\sigma_2\rangle), \\ L_3=-\dfrac{3J_1'}{2kT}(\langle\sigma_1\rangle+\langle\sigma_2\rangle+\alpha\langle\sigma_3\rangle). \end{cases} \quad (A\cdot 4)$$

As in Mekata's two-dimensional model, (A·3) leads to successive phase transitions. For small α we have three ordered phases: (I) $\langle\sigma_1\rangle=-\langle\sigma_2\rangle\neq 0$, $\langle\sigma_3\rangle=0$; (II) $\langle\sigma_1\rangle$, $\langle\sigma_3\rangle$, $\langle\sigma_2\rangle\neq 0$; (III) $\langle\sigma_1\rangle=\langle\sigma_3\rangle>0$, $\langle\sigma_2\rangle<0$. When the temperature is decreased, the transitions (I) $\rightarrow$ (II) $\rightarrow$ (III) occur. For moderate α only (I) and (III) are realized via a first-order transition between (I) and (III). When $|\alpha|$ is increased further, one finally reaches a point where (III) is the only ordered phase.

The temperature dependence of sublattice magnetizations determined by (A·3) and (A·4) is shown in Fig. 5. At $T=T_{N1}$ given by

$$1=\frac{e^{J/kT_{N1}}}{2kT_{N1}}(3J_1'-6J_2'), \quad (A\cdot 5)$$

the paramagnetic state becomes unstable against the phase (I) or the phase (III). The "antiferromagnetic" phase becomes unstable at $T=T_0$, where

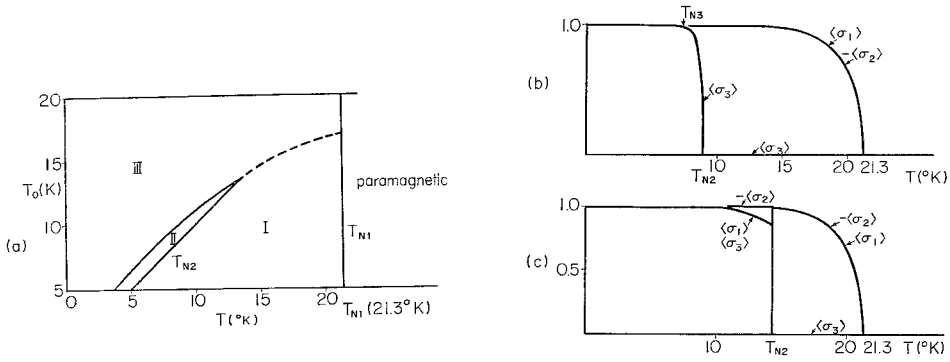

Fig. 5. (a) Phase diagram expected for (A·2). T_{N1} defined by (A·5) is chosen as 21.3°K, which is the experimental value for $CsCoCl_3$. $J=75$°K is used. The temperature T_0 defined in (A·6) is a parameter to show the importance of J_2'. The broken line corresponds to the first-order transition. The other transitions are of second order. (b) The temperature dependence of the order parameters. $J=75$°K, $T_{N1}=21.3$°K and $T_{N2}=T_0=9$°K ($\alpha=-0.0034$) are assumed. (c) The temperature dependence of the order parameters. $J=75$°K, $T_{N1}=21.3$°K and $T_0=14$°K ($\alpha=-0.117$) are assumed.

$$1=\frac{e^{J/kT_0}}{2kT_0}\times(-6J_2'). \tag{A·6}$$

When (II) is present as a stable intermediate phase, T_0 is the second order transition point from (I) to (II), i.e., $T_0=T_{N2}$. However, if the first-order transition occurs from (I) to (III) at $T=T_{N2}$, T_{N2} is higher than T_0.

Identifying T_{N2} as experimental T_{N2} and using $J=75$°K we can estimate J_1' and J_2' for $CsCoCl_3$ as $J_1'/J\sim0.56\times10^{-2}$ and $\alpha\equiv2J_2'/J_1'\sim-0.46\times10^{-2}$. On the other hand, for $CsCoBr_3$ we obtain $J_1'/J\sim0.13\times10^{-1}$ and $\alpha\equiv2J_2'/J_1'\sim-0.6\times10^{-1}$, using $T_{N1}=28.3$°K, $T_{N2}=14$°K and $J=80$°K.

The present theory does not change so much Mekata's picture of the successive phase transitions. The magnitude of interchain coupling estimated above from T_{N1} and T_{N2} is, however, different from the prediction of the two-dimensional model, since we take into account the temperature dependence of correlation length along each chain. The present theory predicts that J_2' is much smaller than J_1'.

References

1) See, for instance,
M. Steiner, J. Villain and C. G. Windsor, Adv. Phys. **25** (1976), 87.
R. J. Birgeneau and G. Shirane, Phys. Today **31** (1978), 32.
2) N. Ishimura and H. Shiba, Prog. Theor. Phys. **63** (1980), 743.
3) J. Villain, Physica **79B** (1975), 1.
4) N. Achiwa, J. Phys. Soc. Japan **27** (1969), 561.
5) W. B. Yelon, D. E. Cox and M. Eibschutz, Phys. Rev. **B12** (1975), 5007.
6) U. Tellenbach and H. Arend, J. Phys. **C10** (1977), 1311.

U. Tellenbach, J. Phys. **C11** (1978), 2287.
7) H. Yoshizawa and K. Hirakawa, J. Phys. Soc. Japan **46** (1979), 448.
K. Hirakawa and H. Yoshizawa, J. Phys. Soc. Japan **46** (1979), 455.
8) W. J. L. Buyers, J. Yamanaka, S. E. Nagler and R. L. Armstrong, Solid State Comm. **33** (1980), 857.
9) S. K. Satija, G. Shirane, H. Yoshizawa and K. Hirakawa, Phys. Rev. Letters **44** (1980), 1548.
H. Yoshizawa, K. Hirakawa, S. K. Satija and G. Shirane, to be published in Phys. Rev. B.
10) See, for example,
H. Fukuyama, R. A. Bari and H. C. Fogedby, Phys. Rev. **B8** (1973), 5579.
M. Saitoh, J. Phys. **C6** (1973), 3255 and references cited therein.
11) W. Breitling, W. Lehmann, T. P. Srinivasan, R. Weber and U. Dürr, Solid State Comm. **24** (1977), 267.
12) W. Breitling, W. Lehmann and R. Weber, J. Magn. Magn. Mat. **10** (1979), 25.
13) I. W. Johnstone and D. J. Lockwood, Solid State Comm. **32** (1979), 285.
14) D. J. Scalapino, Y. Imry and P. Pincus, Phys. Rev. **B11** (1975), 2042.
15) J. D. Johnson, S. Krinsky and B. M. McCoy, Phys. Rev. **A8** (1973), 2526.
16) M. Fowler and M. W. Puga, Phys. Rev. **B18** (1978), 421.
17) M. Date and M. Motokawa, Phys. Rev. Letters **16** (1966), 1111.
18) J. B. Torrance, Jr. and M. Tinkham, Phys. Rev. **187** (1969), 587, 595.
19) M. Mekata, J. Phys. Soc. Japan **42** (1977), 76.
M. Mekata and K. Adachi, J. Phys. Soc. Japan **44** (1978), 806.
20) R. Kubo, *Fuctuation, Relaxation and Resonance in Magnetic Systems*, ed. by ter Haar (Oliver and Boyd, 1962), p. 23.
21) M. Motokawa, J. Phys. Soc. Japan **35** (1973), 1315 and references cited therein.